Supporting information for:

Direct Observation of Charge-Carrier Heating at WZ-ZB InP Nanowire Heterojunctions

Chaw Keong Yong,[†] Jennifer Wong-Leung,[‡] Hannah J. Joyce,[†] Qiang Gao,[‡] James Lloyd-Hughes,[†] H. Hoe Tan,[‡] Chennupati Jagadish,[‡] Michael B. Johnston,[†] and Laura M. Herz[*,†]

Department of Physics, University of Oxford, Clarendon Laboratory, Parks Road, Oxford, OX1 3PU, U.K., and Department of Electronic Materials Engineering, Research School of Physical Sciences and Engineering, Institute of Advanced Studies, Australian National University, Canberra ACT 0200, Australia

E-mail: l.herz@physics.ox.ac.uk

Electron Microscopy and Calculation of Average Nanowire Diameters

Field emission scanning electron microscopy (FESEM) was carried out using a Hitachi S4300 microscope at an accelerating voltage of 5 kV. For each sample, at least 50 individual nanowires were examined. For each individual nanowire, measurements of the nanowire diameter were taken at approximately 250 nm intervals along the entire nanowire length, from which an average diameter

[*]To whom correspondence should be addressed
[†]Department of Physics, University of Oxford
[‡]Department of Electronic Materials Engineering, Australian National University

was calculated. Each nanowire average diameter was then recorded in a histogram bin yielding an average-diameter distribution function for the complete ensemble, as shown in Fig. S1. For each nanowire, the total nanowire length was also measured and for each nanowire ensemble sample, the length- and distribution-averaged nanowire diameter, $< d >$, was then calculated using the formula:

$$< d >= \frac{\sum d_i l_i}{\sum l_i}, \tag{1}$$

where d_i is the average diameter of nanowire i and l_i is its length.

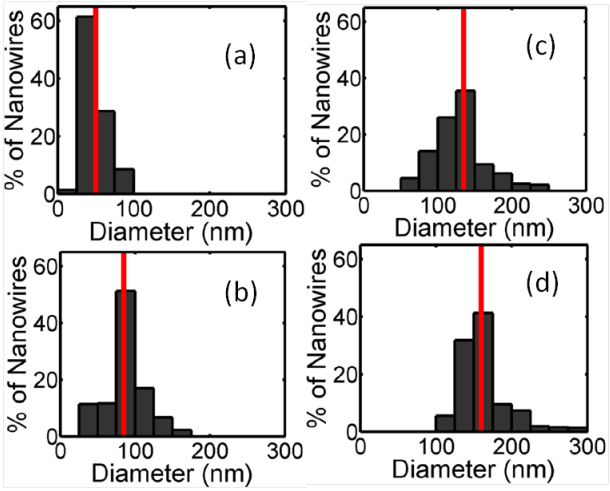

Figure S1: Histograms of the diameters of (a) 50nm-InP NWs, (b) 85 nm, (c) 135 nm and (b) 160nm-InP NWs on quartz.

For transmission electron microscopy (TEM) investigations, nanowires were first mechanically transferred to holey carbon grids. TEM was performed using a Phillips CM300 TEM operated at 300 kV. At least 5 nanowires were examined from each sample. Nanowires were examined for crystal structure and stacking faults over their entire length.

Time-resolved Photoluminescence Spectroscopy

For time-integrated PL measurements, the sample was maintained at a temperature of 77 K in a liquid-nitrogen flow cryostat. Time-resolved PL measurements were performed at room tempera-

ture using a PL up-conversion set-up that has already been described in detail elsewhere.[S1,S2] The sample was excited at a photon energy of 1.68 eV with the output from a mode-locked Ti:Sapphire laser oscillator supplying 100 fs pulses at 82 MHz repetition rate. The PL was gated optically in a β-barium borate crystal using a split-off part of the laser output that was subjected to an adjustable time delay with respect to the excitation pulse. Time-resolved and time-integrated PL spectra were recorded with a liquid-nitrogen cooled CCD detector connected to a spectrometer, and corrected for the spectral response of the apparatus. The spectral resolution of the time-resolved and time-integrated PL systems at the selected detection wavelengths was 32 meV and 4 meV, respectively, and the former system had a time-resolution of 200 fs.

The initial carrier density (n_0) immediately after photoexcitation (t=0) can be calculated from the density of absorbed photons. For the case of the samples under investigation, the nanowires of diameter d=50–160 nm were dispersed lying flat on the substrate. The optical absorption coefficient α at the excitation energy of E_{photon}=1.68 eV is taken from literature values[S3] at 10 K to be 40000 cm^{-1}. The sample is therefore optically thin (i.e. αd=0.2 – 0.6) resulting in the generation of a homogeneous initial carrier density n_0 throughout each individual nanowire given by:

$$n_0 = \frac{f_0}{E_{\text{photon}}} \times \alpha(1-R) \tag{2}$$

Here f_0 is the initial excitation pulse fluence incident on the nanowire and R accounts for the reflection losses occurred at the InP interface, given by $R=(n-1)^2/(n+1)^2 \sim 0.26$ with n=3.1.[S4]

The initial excitation fluence f_0 experienced by the nanowires is given by that at the very centre of the Gaussian excitation spot profile because of the experimental conditions used, as described in the following. The excitation spot on the sample had a full-width-at-half maximum of w=240 μm, which generated emission that was imaged with two off-axis parabolic mirrors onto the nonlinear crystal with a magnification ratio of 4.1. The PL image of 1 mm diameter was then optically gated with a gate beam of 80 μm diameter. Therefore, this set-up probes an excitation area of diameter only $0.08w$ with respect to the overall excitation spot. The probed emission as a result is highly

homogenous as it is generated by the fluence f_0 at the very centre of the Gaussian excitation spot, given by

$$f_0 = \frac{\sqrt{2}P}{\pi\left(\frac{w}{2}\right)^2} r_{\mathrm{rep}}, \tag{3}$$

where P is the time-averaged total excitation power incident on the sample surface and r_{rep}=82 MHz is the pulse repetition rate of the excitation laser. Overall, this system of measurement therefore ensures that a well-defined and uniform volume density of carriers is generated in the ensemble of nanowires probed.

Terahertz Time-Domain Spectroscopy

The optical pump terahertz probe measurements were conducted on the experimental setup that has been described previously.[S5] An amplified Ti:Sapphire laser with 4 W average power was used to generate 35 fs pulses centred at 800 nm at a 5 kHz repetition rate. Each pulse was split into three paths: approximately 590 μJ/pulse was used as the optical pump to photoexcite the sample, 200 μJ/pulse was used to generate the THz probe pulse via optical rectification in a 2 mm GaP crystal, and 1.6 μJ/pulse was used as a gate for electro-optic detection of the transmitted THz pulse with a 200 mm GaP crystal. The optical pump beam was attenuated using neutral density filters to produce sample photoexcitation fluences between 1 and 160 μJ/cm^2. At the sample, the optical pump beamwidth had a full width at half maximum (FWHM) of 13 mm, whereas the THz probe FWHM was only 1.3 mm. Therefore the terahertz probe measured an area of approximately constant photoexcited carrier density. The THz electric field, E, was detected using a balanced photodiode circuit, and the signal was extracted using a lock-in amplifier referenced to a 2.5 kHz chopper in the THz generation beam. A second lock-in amplifier was used to detect the optical pump-induced change in terahertz electric field, ΔE, by referencing to a 125 Hz chopper in the optical pump beam. Varying the delay between the optical pump, terahertz probe and optical gate pulse produced a two-dimensional map of the THz spectral response of the material as a function of time after photoexcitation. The measurements were performed at room temperature with the entire

terahertz beam path under vacuum, to avoid absorption of the terahertz radiation by atmospheric water vapour.

Electron Quantum Confinement Energy Calculation

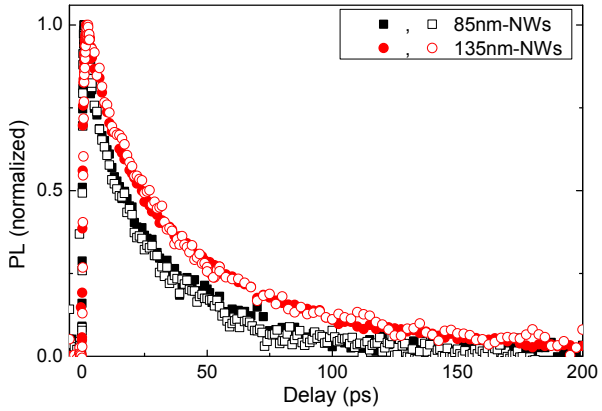

Figure S2: Single particle energy in the superlattices plane for the first electron in the WZ-ZB-WZ quantum well with different well-width.

The electronic eigenstates for a single wurtzite InP quantum well in zinc blende InP were calculated for various well widths L. A conduction band discontinuity of 129 meV and an electron effective mass of $0.08\,m_e$ (in well and barrier) were assumed. Figure S2 shows the energies of the two lowest eigenstates E_1 and E_2 with respect to the wurtzite conduction band minimum, as a function of well width. One bound state is found in the range $L > 0.8$ nm, and a second bound state appears when $L > 6.2$ nm. The increase in the PL emission energy resulting from quantum confinement is dominated by electron confinement in the zinc blende wells. The majority of the hole population will be located in the wurtzite section, with negligible confinement energy.

Time-Integrated PL Spectral Maps of 85nm and 135nm InP NWs

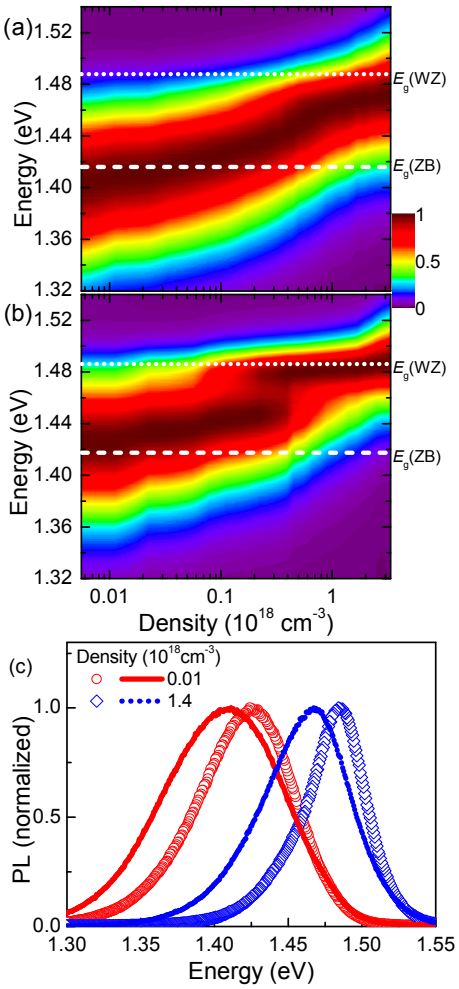

Figure S3: TIPL spectra maps for (a) 85 nm-InP NWs and (b) 135 nm-InP NWs showing the intensity (on a linear false colour scale) as a function of initial charge injection density (horizontal scale) and emission energy (vertical scale). For clarity, all spectra were normalized to their maximum intensity. The dotted and dashed lines indicate the bandgap energy of the WZ phase (E_g(W)) and the ZB phase E_g(ZB) at 77 K, respectively. (c) Individual TIPL spectra for 85 nm-InP NWs (dotted and dotted lines) and 135 nm-InP NWs (circles and diamonds), displaying the evolution of the PL spectra as the initially injected charge carrier density is increased from 1×10^{16} cm^{-3} to 1.4×10^{18} cm^{-3}.

Transient PL of 85nm and 135nm InP NWs

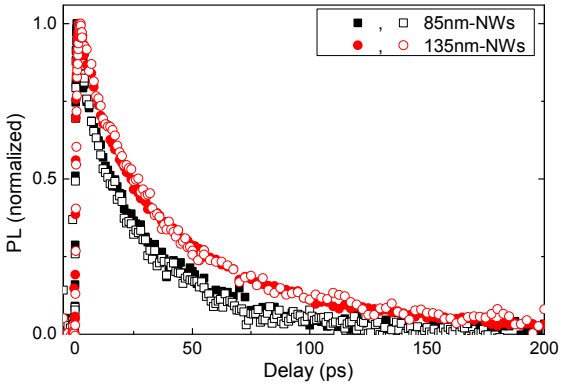

Figure S4: Transient photoluminescence (PL) decays of InP NWs measured at 300 K as a function of time after excitation. Thes nanowires were excited at a photon energy of 1.68 eV with pulse fluences generating an initially injected charge carrier density of 1.4×10^{18} cm^{-3} (empty symbols) and 0.7×10^{18} cm^{-3} (solid symbols). The PL emission was detected at the energy corresponding to the bandgap of the WZ phase (1.44 eV).

Carrier Cooling curves for 85nm and 135nm InP NWs

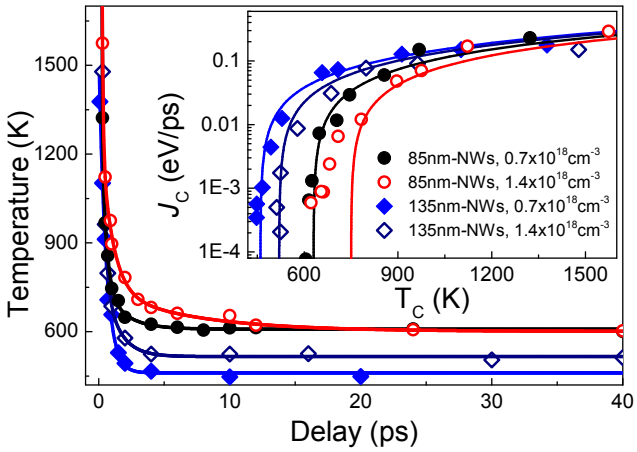

Figure S5: Charge carrier temperature at substrate temperature of 300 K, plotted as a function of time delay for 85 nm-InP NWs (circle) and 135 nm-InP NWs (diamond), as extracted from exponential fitting to the high-energy tail of the corresponding PL spectra. The inset shows the energy loss rate of hot carriers (J_c) plotted as a function of carrier temperature T_c, extracted from the cooling curves in for 85 nm-NWs (circle) and 135 nm-NWs (diamond) through numeric differentiation. The solid and empty symbols show the energy loss rate obtained at initial charge carrier densities of 1.4×10^{18} cm^{-3} and 0.7×10^{18} cm^{-3}, respectively. The solid lines are guides to the eye.

Acoustic (AC) Phonon Cooling

We may rule out the possibility of diameter-dependent nanowire cooling causing the changes in charge carrier cooling rate for nanowire ensembles with different average diameter. Non-equilibrium filling of AC phonon modes has generally been observed in bulk semiconductors for photoexcitation densities above $10^{18}\,\mathrm{cm}^{-3}$.[S6] The cooling of such AC phonon distributions, on the other hand, is controlled by the heat-diffusion limited interaction with the surroundings.[S7] Such heat transfer to the substrate environment has been shown to depend on the dimension and the surrounds of the nanostructure.[S7,S8] In this simple model, the heat diffusion time constant (τ_D) in a semiconductor nanostructure is given by $\tau_\mathrm{D} = \frac{C_p \rho_p R^2}{9 C_m \rho_m \Lambda}$, where R is the radius, C is the specific heat, ρ is the density, and Λ is the linear thermal conductivity for the nanoparticle p in the surrounding matrix m. For the study presented here, nanowires were dispersed flat on quartz substrates, hence the heat dissipation is dominated by the radial diffusion from the nanowires to the substrate, which ought to be more effective for nanowires with smaller diameter. We estimate a diffusion cooling time of $\approx 478\,\mathrm{ps}$ and $4820\,\mathrm{ps}$ for 50nm-InP NWs and 160nm-InP NWs, respectively, under our experimental conditions (based on established parameters:[S9] $\mathrm{C_{InP}} = 45.4\,\mathrm{Jmol^{-1}K^{-1}}$, $\mathrm{C_{quartz}} = 45.3\,\mathrm{Jmol^{-1}K^{-1}}$, $\rho_\mathrm{InP} = 4.81\,\mathrm{gcm^{-3}}$, $\rho_\mathrm{quartz} = 2.20\,\mathrm{gcm^{-3}}$, $\Lambda_\mathrm{quartz} = 0.013\,\mathrm{Jcm^{-1}K^{-1}s^{-1}}$). These heat diffusion times are much longer than the times scales involved in the rapid charge-carrier cooling through exchange with phonon modes and, as a result, a sizeable non-equilibrium phonon distribution is able to build up, as described in the main text. The simple model of heat diffusion outlined here would suggest that the acoustic phonon bottleneck is resolved faster in the thinner nanowires, as these will have more effective heat conduction to the substrate. In contrast, we actually observe consistently higher charge carrier temperatures in the smaller-diameter nanowires. These observations strongly suggest that the charge cooling dynamics are in fact dominated by the additional carrier heating induced by charge transfer across heterojunction interfaces, which occur in higher density for the thinner nanowires.

References

(S1) Schmid, S. A.; Abbel, R.; Schenning, A. P. H.; Meijer, E. W.; Sijbesma, R. P.; Herz, L. M. *J. Am. Chem. Soc.* **2009**, *131*, 17696.

(S2) Yong, C. K.; Joyce, H. J.; Lloyd-Hughes, J.; Gao, Q.; Tan, H. H.; Jagadish, C.; Johnston, M. B.; Herz, L. M. *Small* **2012**, *8*, 1725–1731.

(S3) Palik, E. D. *Handbook of Optical Constants of Solids*; Academic Press: New York, 1985.

(S4) Adachi, S. *J. Appl. Phys.* **1989**, *66*, 6030.

(S5) Parkinson, P.; Joyce, H. J.; Gao, Q.; Tan, H. H.; Zhang, X.; Zou, J.; Jagadish, C.; Herz, L. M.; Johnston, M. B. *Nano Lett.* **2009**, *9*, 3349–3353.

(S6) Klimov, V.; Bolivar, P. H.; Kurz, H. *Phys. Rev. B* **1995**, *52*, 4728–4731.

(S7) Ge, Z.; Cahill, D. G.; Braun, P. V. *J. Phys. chem. B* **2004**, *108*, 18870–18875.

(S8) Achermann, M.; bartko, A. P.; Hollingsworth, J. A.; Klimov, V. I. *Nat. Phys.* **2006**, *2*, 557–561.

(S9) Yu, P. Y.; Cardona, M. *Fundamentals of semiconductors*; Springer-Verlag: Heidelberg, 1996.